

## On estimation of coastal wave parameters and wave-induced shear stresses

J. Xiong <sup>1</sup>, Y. P. Wang <sup>1,2,3\*</sup>, S. Gao <sup>2</sup>, J. Du <sup>4,5</sup>, Y. Yang<sup>1</sup>, J. Tang<sup>1</sup>, J. Gao <sup>1</sup>

<sup>1</sup>Ministry of Education Key Laboratory for Coast and Island Development, Nanjing University, Nanjing, China

<sup>2</sup>State Key Laboratory of Estuarine and Coastal Research, School of Marine Sciences, East China Normal University, Shanghai, China

<sup>3</sup>School of Geographic and Oceanographic Sciences, Nanjing University, Nanjing, China

<sup>4</sup>Virginia Institute of Marine Science, Gloucester Point, Virginia

<sup>5</sup>Texas A&M University at Galveston, Galveston, Texas

### Abstract

Wave parameters, e.g., wave height, near-bed wave orbital velocity, and wave-induced shear stresses, are important hydrodynamic parameters for sediment processes in coastal oceans. Wave orbital velocity is particularly critical in sediment resuspension. Several algorithms to calculate wave orbital velocity have been proposed, including linear wave theory, spectrum, and Joint North Sea Wave Project methods, but the validity of these algorithms in relatively shallow waters is not well understood. In this study, we compared the wave parameters obtained by different instruments and algorithms at four sites, one within the intertidal zone with a mean depth of 1 m and the remainder three in deeper offshore water with mean depths of 15–30 m. We found a high consistency of the estimated wave height, peak wave period, and wave orbital velocity among different datasets and different algorithms at the offshore sites, while there were significant discrepancies at the shoreline site. Using *Ursell number*, our study suggests that it is reliable to apply any of the three algorithms and different instruments (acoustic Doppler velocimeter and buoy) in deeper water. However, for very shallow water, it is recommended to use the measured high-frequency velocity and spectrum method to calculate wave orbital velocity, and use wave gauge instrument or zero-crossing algorithm to obtain wave height and period information. Finally, the effect of turbulence and bedform morphology on wave-induced shear stress is discussed: without removing the turbulence or taking into account bedforms (e.g., ripples), the orbital velocity will be remarkably over-estimated or under-estimated.

Wave orbital velocity ( $U_w$ ) and wave-induced shear stress ( $\tau_w$ ) are important parameters for coastal engineering projects (e.g., port development and beach nourishment) as they greatly regulate sediment transport in coastal waters (Wiberg and Sherwood, 2008). Sediment erosion, transport, and deposition are largely controlled by bottom shear stress. Unlike the current-induced shear stress, which can be calculated in relatively simple ways (e.g., inertial dissipation, Reynolds stress, and turbulence kinetic energy) (Kim et al., 2000; Biron et al., 2004), the wave-induced shear stress is difficult to obtain directly from flow measurements within the thin wave boundary layer. It is usually determined by the bottom wave orbital velocity ( $U_w$ ) and wave friction factor ( $f_w$ ) (Soulsby, 1997). However, it is still a challenge to estimate accurately the wave orbital velocity and friction factor.

Several algorithms to calculate  $U_w$  have been summarized in Wiberg and Sherwood (2008), but their validity has not yet

been well understood for different water depths, especially in very shallow waters. The most widely used algorithm to calculate wave orbital velocity is based on the simple linear wave theory (Soulsby and Smallman, 1986; Soulsby, 1987; Zhu et al., 2016; Yu et al., 2017). Errors arise when only particular statistical parameters such as significant wave height ( $H_s$ ) and peak period ( $T_p$ ) rather than the full wave spectrum are utilized. Another way to calculate  $U_w$  is to integrate the contributions of each frequency component of near-bed high-frequency velocity (i.e., the spectrum method). Even without the near-bed velocity measurement,  $U_w$  can still be estimated by approximating a generic surface-wave spectrum using known values of wave height and period (Wiberg and Sherwood, 2008). Compared with other semi-empirical wave spectra forms, Joint North Sea Wave Project (JONSWAP) (Hasselmann et al., 1973; Donelan et al., 1985) is most appropriate for sediment transport in the shallow waters, as it includes the impact of wave interaction with bottom sediment (Soulsby, 1997).

\*Correspondence: ypwang@nju.edu.cn

In addition to the impact of wave orbital velocity, influence from bedforms on shear stress calculation should be carefully considered. The presence of bedforms is very important in modulating the bottom stress, near-bed turbulence, and sediment entrainment (Bolaños et al., 2012). Such bedforms cover a broad range of scales (e.g., ripples, mega-ripple, sand waves, and tidal ridges), but only those whose length scales are on the same order of magnitude of the wave orbital diameter near the bed contribute to bottom shear stress (Van Rijn, 2007). The presence of ripples modifies bottom roughness height and wave friction factor, and exerts significant influence on wave-induced shear stress (Soulsby, 1997). According to Gao (2009) and Zhao et al. (2012), ripples with a wavelength of several centimeters and a wave height <1 cm are ubiquitous on Jiangsu tidal flats. Their influences on bottom shear stress and sediment transport have not been reported yet. On a rippled bed, the total wave-induced bed shear stress ( $\tau_w$ ) is composed of a skin-friction component ( $\tau_{ws}$ ) and a ripple component ( $\tau_{wr}$ ) (Soulsby, 1997). In terms of sediment transport,  $\tau_{ws}$  is responsible for bedload transport and threshold of sediment motion from the bed, and  $\tau_{wr}$  contributes to upward turbulence diffusion of near-bed suspended sediment (Soulsby, 1997). Due to their importance in hydrodynamic and sediment processes, many studies have been conducted to measure and predict the dimension, formation and type of ripples through laboratory experiments and field measurements (Grant and Madsen, 1982; Li and Amos, 1998; Davis et al., 2004; Soulsby and Whitehouse, 2005; Bolaños et al., 2012). Li and Amos (2001) proposed an empirical formula to estimate the ripple wavelength and wave height, and to calculate  $\tau_{wr}$  based on ripple-enhanced roughness height  $k_{br}$ .

In this paper, we calculated and compared wave orbital velocities on the basis of in situ measurements using different methods. The purposes of this contribution are to (1) examine the validity of each algorithm (i.e., linear wave theory, spectrum, and JONSWAP methods) for both shallow and deep water areas; (2) investigate the effects of turbulence on wave orbital velocity estimation; and (3) examine the impact of bedforms on the wave-induced shear stress, proposing suggestions for accurate estimation of bottom shear stress.

### Study area

We conducted a systematic and high-frequency in situ measurements in both shallow and deep waters off the Jiangsu Coast and Zhejiang Coast (Fig. 1). The Jiangsu Coast is adjacent to the Yellow Sea (YS), while the Zhejiang Coast is close to the East China Sea (ECS). YS and ECS are part of the western Pacific marginal sea, with the former being a semi-enclosed sea with a mean depth of 44 m and the latter being connected to YS in the north, representing a broad continental shelf and a mean depth of 72 m (Dong et al., 2011). One-year buoy measurements in the southern part of YS show that the local significant wave height ranges from 0.15 to 2.22 m,

with an average of 0.59 m. The average wave period is in the range of 2.06–6.82 s (Yang et al., 2014). The dominant wind direction is from the north in winter and from the south in summer, with an average speed of 2.8–4.4 m s<sup>-1</sup> (He et al., 2010). Cold outbreaks in winter and typhoons in summer are major natural hazards to the coastal engineering (Yang et al., 2014). In ECS, waves are stronger in winter, with a monthly mean wave height of 1.1–1.3 m; waves from April to June are weaker, with a mean wave height of 0.9 m (Dong et al., 2011).

## Methods

### Data collection

Multiple datasets for several tidal cycles were collected at four stations (Fig. 1), with one in the intertidal zone (T1, on the upper-middle part of the intertidal flat on the Jiangsu Coast) and three in deeper water areas (W1, X1, and S1). A tripod observation system was deployed at station T1 to continuously measure waves and tides. A SBE 26plus Wave and Tide Recorder were deployed at 0.1 m above bed, monitoring pressure for 256 s at 4 Hz at a 10 min burst interval. Three-dimensional and high-frequency (8 Hz) velocities at 0.2 m

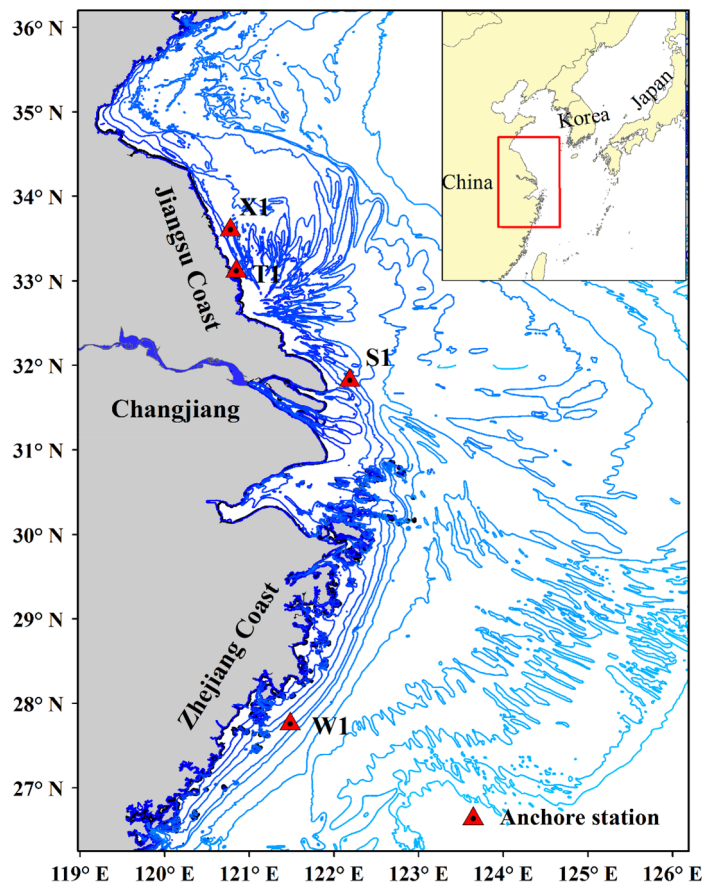


**Fig. 1.** Map showing the study area and observational sites along Jiangsu coast and Zhejiang coast of China.

**Table 1.** Summary of instrumentation and deployment period of observation stations.

Stations	Location	Instrumentation						Deployment time
		ADV		SBE 26plus		Buoy		
		Sampling frequency/ burst interval/ samples per burst	Velocity sampling height	Sampling frequency/ burst interval/ samples per burst	Deployment height	Sampling frequency/ burst interval/ samples per burst	Deployment height	
T1	33°09.288'N 120°50.752'E	8 Hz/1 min/240	0.20 mab	4 Hz/10 min/1024	0.1 mab	/	/	27 Apr– 2 May 2013
W1	27°47.670'N 121°29.007'E	16 Hz/30 min/8192	0.30 mab	/	/	4 Hz/1 h/1200	Sea surface	17 Feb–13 Mar 2014
X1	33°38.613'N 120°46.623'E	16 Hz/10 min/4096	0.35 mab	/	/	4 Hz/1 h/1200	Sea surface	29 Dec 2014– 10 Jan 2015
S1	31°51.586'N 122°11.104'E	16 Hz/20 min/8192	0.30 mab	/	/	4 Hz/30 min/1200	Sea surface	20 Dec 2015– 19 Jan 2016

mab: meter above bottom

above bed were measured by a 6 MHz Nortek Acoustic Doppler Velocimeter (ADV) for 30 s in each burst interval of 1 min. At the offshore stations W1, X1, and S1, the WatchKeeper buoy from AXYS Technologies, Canada, was deployed to measure wave parameters. The buoy is equipped with AXYS TRIAXYS OEM wave measurement modules and wave information (mean, maximum, and significant wave height; mean wave direction; mean wave period; and wave direction spread) was evaluated by the TRIAXYS processing system with three accelerometers (TRIAXYSTM OEM Directional Wave Sensor user's manual, 2009; Wilson and Siegel, 2011; MacIsaac and Naeth, 2013). The wave surface elevations were recorded by buoy for duration of 10 min in every 1 h. We also deployed a near-bed tripod observation system at each offshore station, with ADV recording at 16 Hz at 0.30 m (stations W1 and S1) or 0.35 m (station X1) above the bed. The quality of the collected data by ADV was examined by vector correlations and signal-to-noise ratio, then by properly despiking to exclude outliers. The outliers were replaced by the values from cubic interpolation (Goring and Nikora, 2002; Lu et al., 2012). Using the PUV algorithm (P: pressure; U: east-velocity; V: north-velocity, referred to as ADV-PUV in the subsequent text) (Wu et al., 1996; Sobey and Hughes, 1999; Gordon and Lohrmann, 2002), we extracted wave parameters (e.g., peak period and significant wave height) from water pressure and current velocity data recorded by ADV. Subsequently, the estimated wave height and peak wave period by ADV-PUV algorithm were cross-checked with a SBE 26plus data for the intertidal station and buoy data for the offshore stations, respectively. Further, sediment samples were collected near the tripod deployment sites. Grain size parameters were analyzed using a Malvern Mastersizer 2000 laser granulometer (requiring sediment samples in the size range of 0.02–2000 μm). The median grain sizes of bottom sediment were 70.4 and 14.3 μm for stations T1 and S1, respectively. Details of the stations, including longitude/latitude, sampling frequency, sensor elevations, and deployment time, are listed in Table 1.

**Wave orbital velocity  $U_w$**

*Estimation of  $U_w$  by linear wave theory*

Simple linear wave theory is most frequently used to estimate wave orbital velocity because of its simplicity in mathematical derivation. For small-amplitude, monochromatic (single frequency) waves, linear wave theory defines the amplitude of the wave orbital velocity  $U_{w\_Linear}$  as

$$U_{w\_Linear} = \frac{\pi H}{T \sin h(kh)} = \frac{\pi H_s / \sqrt{2}}{T_p \sin h(kh)} \quad (1)$$

where  $h$  is water depth,  $k$  ( $=4\pi^2/[gT^2 \tanh(kh)]$ ) is the wave number solved through an iterative process,  $H$  is wave height and  $T$  is wave period. To calculate wave-induced shear stress, a representative monochromatic wave is chosen. A good choice

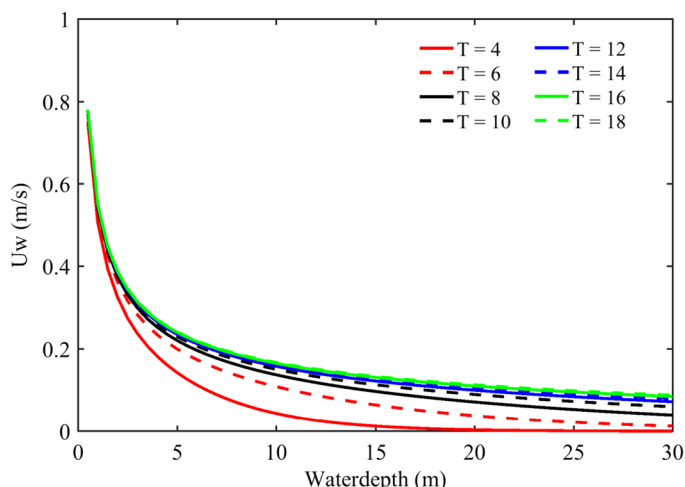


**Fig. 2.** Wave orbital velocity  $U_w$  as a function of water depth for period ranging from 4 to 18 s.  $H_s$  is assumed as 0.5 m.

for this is the wave of significant height  $H_s (= \sqrt{2}H)$  and peak period  $T_p (=T)$  (Soulsby, 1997).  $H_s$  and  $T_p$  are deduced using ADV-PUV algorithm.

According to Wiberg and Sherwood (2008), wave orbital velocity calculated using linear wave theory was in good agreement with observed oscillatory flows under monochromatic wave except within the wave boundary, where the frictional effects cannot be ignored and velocities increase with height

above the bottom from 0 to  $U_w$ . However, waves in the sea are usually not monochromatic and they often consist of different heights, periods, and directions, limiting the capability of the linear wave theory. As shown in Fig. 2, the increase in  $U_w$  with increasing  $T$  is unapparent in shallow water (water depth <1 m), but the differences become more pronounced as water depth increases. That means longer period waves affect water column to much greater depths than those with shorter periods. With increasing water depth, low-frequency (long period) components of the wave spectrum contribute disproportionately to the bottom orbital wave motions while higher-frequency (short period) wave motion may be completely attenuated before reaching the bottom. Therefore, only when the water is shallow with respect to the wavelength of the waves can the single measure of wave height and period used in Eq. 1 capture the contribution of full wave spectrum to bottom orbital velocity. Otherwise, we recommend using every wave height and wave period of each burst to obtain wave orbital velocity.

**Estimation of  $U_w$  by spectrum method**

Wave motions dominate bottom velocity spectrum over periods ranging from a few to tens of seconds. By deploying high-frequency sampling instruments (e.g., ADV), near-bottom velocity in both low-frequency (e.g., tides and wind-driven currents) and high-frequency (turbulence) can be obtained. Relating bottom orbital velocity directly to the

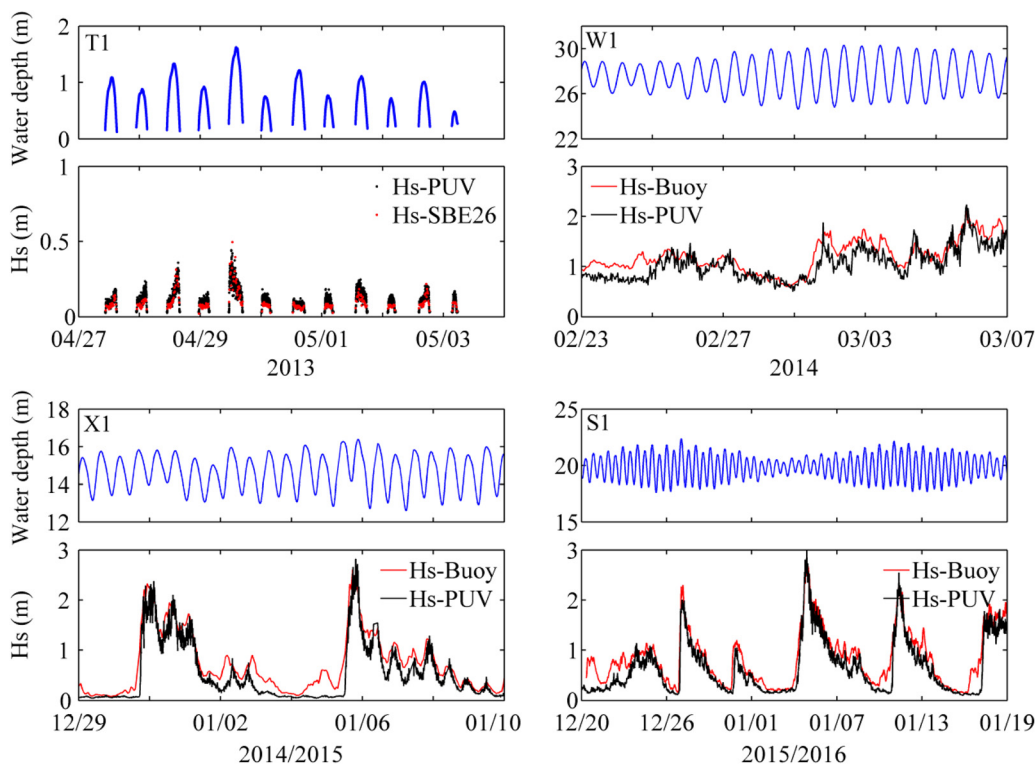


**Fig. 3.** Water depth and significant wave height obtained by PUV algorithm and SBE 26plus at intertidal station T1, by PUV algorithm and buoy at offshore stations W1, X1 and S1.

**Table 2.** Water depth (m), significant wave height  $H_s$  (m), peak wave period  $T_p$  (s), wave orbital velocity  $U_w$  ( $m\ s^{-1}$ ) and wave-induced shear stress  $\tau_w$  ( $N\ m^{-2}$ ). Values included in the brackets are the average value of each parameter.

Stations	$H_s$			$T_p$			$U_w$			$\tau_w$		
	Water depth	ADV (PUV)	SBE 26plus	Buoy	ADV (PUV)	Buoy	Spectrum	Linear	JONSWAP	$\tau_{ws}$	$\tau_{ws\_van}$	$\tau_{ws\_GM}$
T1	0-1.62 (0.77)	0.03-0.44 (0.12)	0.02-0.50 (0.10)	/	1.07-10.03 (3.33)	/	0.02-0.38 (0.09)	-0-0.31 (0.07)	/	-0-0.68 (0.07)	0.03-2.49 (0.52)	0.04-1.56 (0.39)
S1	17.60-22.37 (19.82)	0.10-3.00 (0.67)	/	0.14-2.78 (0.86)	5.09-9.09 (6.25)	1.80-11.1 (5.94)	0.01-0.33 (0.07)	0.01-0.38 (0.06)	-0-0.35 (0.07)	-0-0.43 (0.03)	-0-0.80 (0.07)	-0-0.54 (0.11)
W1	24.62-30.31 (27.59)	0.50-2.50 (1.14)	/	0.60-2.10 (1.30)	5.86-1 (1.37)	3.80-11.10 (7.56)	0.04- (0.10)	0.02-0.25 (0.10)	-0-0.22 (0.09)	/	/	/
X1	12.59-16.39 (14.62)	0.03-2.82 (0.50)	/	0.08-2.61 (0.68)	5.17-13.50 (7.12)	1.60-13.30 (5.78)	-0-0.51 (0.09)	-0-0.54 (0.08)	-0-0.44 (0.08)	/	/	/

variance of wave-induced near bed velocity (Wiberg and Sherwood, 2008),  $U_w$  was calculated by integrating the contributions of each frequency component of  $S_{uv,i}$

$$U_{w\_Spectrum} = \sqrt{2 \sum_i S_{uv,i} \Delta f} \quad (2)$$

where  $S_{uv} = S_{uu} + S_{vv}$  is the combined horizontal spectrum of eastern and northern velocity. In addition, turbulence influence shall be removed (Soulsby and Humphery, 1990; Zhu et al., 2016), or the orbital velocity would be highly overestimated. Since the frequency of turbulence and wave interact with each other (Bricker and Monismith, 2007), the influence of turbulence cannot be totally removed due to the limitation of the method.

#### Estimation of $U_w$ by JONSWAP method

If measurements of high-frequency near-bed velocity and pressure data are not available, then a solution to the estimation of wave orbital velocity is to approximate the surface-wave spectrum with a generic surface-wave spectrum using known values of wave height and period, then use this estimated spectrum to calculate bottom orbital velocity (Wiberg and Sherwood, 2008). A number of general forms for wind-generated wave spectra have been proposed, including Pierson and Moskowitz (1964) spectrum, the JONSWAP spectrum (Hasselmann et al., 1973), and modified JONSWAP (Donelan et al., 1985). Among these spectra forms, JONSWAP is the most appropriate algorithm to calculate wave orbital velocity for sediment transport studies, because it can be applied to shallow water environments:

$$S_{\eta}(f) = \frac{m_0 f_p^4 \chi}{f^5} \left( \frac{f}{f_p} \right)^{\xi} \exp \left[ -\beta \left( \frac{f}{f_p} \right)^{-4} \right] \gamma \exp \left[ -(f-f_p)^2 / (2\sigma^2 f_p^2) \right] \quad (3)$$

$$S_{u,i} = \frac{4\pi^2}{T_i^2 \sin^2(k_i h)} S_{\eta,i} \quad (4)$$

$$U_{w\_JONSWAP} = \sqrt{2 \sum_i S_{u,i} \Delta f_i} \quad (5)$$

$$f_p = 1/T_p \quad (6)$$

$$H_s = 4\sqrt{m_0} = 4\sqrt{\int S_{\eta}(f) df} \quad (7)$$

where  $m_0$  is the variance of water surface elevation,  $f_p$  is peak frequency,  $\zeta$ ,  $\beta$ ,  $\sigma$ ,  $\gamma$ , and  $\chi$  are parameters that adjust the magnitude and shape of JONSWAP spectrum. Interpretations about these parameters used in Eqs. 3-7 can be found in Wiberg and Sherwood (2008).

#### Wave friction factor

Wave-induced shear stress, obtained from wave orbital velocity and wave friction factor ( $\tau_w = \frac{1}{2} \rho f_w U_w^2$ ; Soulsby, 1997), is the most important hydrodynamic property of waves for

sediment transport. The presence of ripples modifies bottom roughness height and wave friction factor  $f_w$ , which in turn influence wave-induced shear stress (Soulsby, 1997; van Rijn, 2007). Wave friction factor was calculated according to Jonsson (1967), as modified by Nielsen (1979):

$$f_w = \begin{cases} \exp\left[5.213(k_b/A_b)^{0.194} - 5.977\right], & A_b/k_b > 1.7 \\ 0.28, & A_b/k_b \leq 1.7 \end{cases} \quad (8)$$

where  $A_b (=U_w T/2\pi)$  is the near-bed wave orbital amplitude,  $k_b$  is the bottom roughness height. Usually,  $k_b$  is expressed as grain size roughness height or Nikuradse roughness height  $k_g (=2.5d_{50})$  (Nielsen, 1992; Soulsby, 1997; Zhu et al., 2016), which was introduced by Nikuradse (1932) to simulate the hydraulic roughness of arbitrary roughness elements of the bottom boundary. To investigate the effect of ripples on wave-induced shear stress, the ripple-related roughness height ( $k_{br\_van}$ ) is calculated as (van Rijn, 2007)

$$k_{br\_van} = \begin{cases} 150f_{cs}d_{50}, & \psi \leq 50 \text{ (lower wave-current regime, small-scale ripples)} \\ 20f_{cs}d_{50}, & \psi > 250 \text{ (upper wave-current regime; sheet flow)} \\ (182.5 - 0.652)\psi f_{cs}d_{50}, & 50 < \psi \leq 250 \text{ (transitional regime; linear approach)} \\ 20d_{silt}, & d_{50} < d_{silt} \end{cases} \quad (9)$$

where  $\psi (=U_{wc}^2/[(s-1)gd_{50}])$ ,  $(U_{cw})^2 = (U_w)^2 + (U_c)^2$  is current-wave mobility parameter;  $s = \rho_s/\rho_w$ ,  $\rho_s$  is the density of primary particle ( $=2650 \text{ kg m}^{-3}$ );  $d_{silt} = 32 \text{ }\mu\text{m}$ ;  $f_{cs} = (0.25d_{gravel}/d_{50})^{1.5}$ ;  $f_{cs} = 1$  for  $d_{50} \leq 0.25d_{gravel}$ ; and  $d_{gravel} = 0.002 \text{ m}$ . The low limit is  $k_{br\_van} = 20d_{silt}$  for particles  $\leq 32 \text{ }\mu\text{m}$ .

A number of formulae have been proposed to predict ripple morphology, based on laboratory experiments and field measurements (Allen, 1970; Grant and Madsen, 1982; Boyd et al., 1988; Williams et al., 2005; Soulsby and Whitehouse, 2005). However, there is still a high degree of scatter in these predictions, particularly when associated with field observations (Bolaños et al., 2012). According to Soulsby (1997), the ripple length  $\lambda$  is typically between 1.0 and 2.0 times of the orbital amplitude of the wave motion at the bed, and their height  $\eta$  is typically between 0.1 and 0.2 times of their length, the ripple length  $\lambda$  associated with waves is given according to Boyd et al. (1988)

$$\lambda = 557A_b(U_w A_b/\nu)^{-0.68} \quad (10)$$

The ripple height  $\eta$  was predicted by Allen (1970)

$$\eta = 0.074\lambda^{1.19} \quad (11)$$

The predicted ripple dimensions are used to obtain the ripple roughness height  $k_{br\_GM}$  (Grant and Madsen, 1982)

$$k_{br\_GM} = 27.7\eta^2/\lambda \quad (12)$$

Accordingly, the grain size roughness height  $k_g$  was used to calculate skin-friction wave shear stress  $\tau_{ws}$ , while the form-related bed shear stress ( $\tau_{wr\_van}$  and  $\tau_{wr\_GM}$ ) was defined from ripple-related roughness height ( $k_{br\_van}$  and  $k_{br\_GM}$ ). To assess whether or not ripples exist under strong hydrodynamic conditions, the skin-friction shear velocity  $\tau_{ws}$  was used to compare with the critical shear stress  $\tau_{up}$  for sheet-flow transports. If  $\tau_{ws} > \tau_{up}$ , then upper-plane bed sheet-flow occurs and ripples are completely washed out. The  $\tau_{up}$  value was calculated by (Li and Amos, 2001)

$$\tau_{up} = \theta_{up}(\rho_s - \rho_w)gd_{50} \quad (13)$$

$$\theta_{up} = 0.172d_{50}^{-0.376} \quad (14)$$

where  $\theta_{up}$  is the critical Shields parameter for sheet flow. The parameter  $d_{50}$  in Eq. 14 has a dimension of cm.

## Results

### Wave parameters measured by different instruments

Water depth and significant wave height over the entire observation period of all stations are presented in Fig. 3. The average water depth was 0.8 m at T1, 27.6 m at W1, 14.6 m at X1 and 18.9 m at S1. The pattern of the varied tidal range indicates the characteristics of mixed semidiurnal tides on the Jiangsu and Zhejiang coasts. The tides were approximately symmetrical in the study area (Fig. 3).

Significant wave height  $H_s$  and peak period  $T_p$  obtained by ADV-PUV algorithm, SBE 26plus and buoy were listed in Table 2. The peak periods obtained from SBE 26plus at T1 were below 1 s, which was erroneous for waves on the tidal flat, where the typical wave period was 1–10 s; thus,  $T_p$  by SBE 26plus was not considered for further analysis.

Waves were mainly caused by local winds in our study area. The average wave period was 3.33 s (by ADV-PUV algorithm) at station T1, and the estimated wave periods by ADV-PUV algorithm and by buoy at offshore stations were close to each other. The similarity between  $H_s$  obtained from ADV-PUV algorithm and buoy indicates that ADV-PUV algorithm is robust to obtain wave parameters at all offshore stations. At T1, however, the values of  $H_s$  estimated by ADV-PUV algorithm were greater than those measured by SBE 26plus, particularly when maximum water depth  $< 1 \text{ m}$  (Fig. 3). This is mainly due to the nonlinear properties of

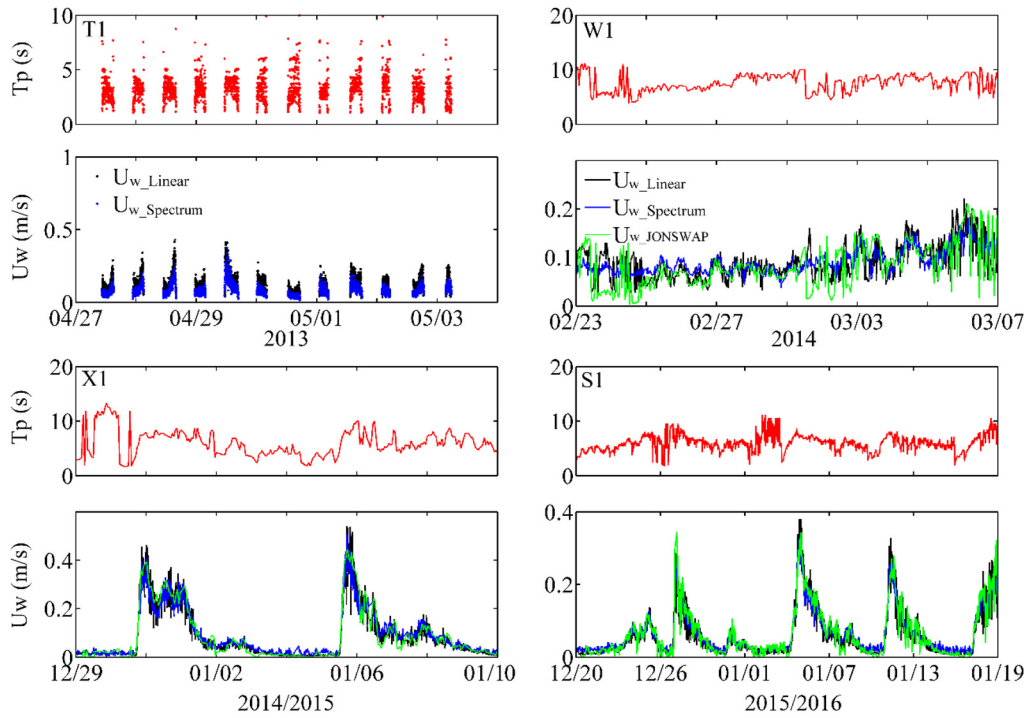


**Fig. 4.** Peak period ( $T_p$ ) and comparison among wave orbital velocity calculated by linear wave theory ( $U_{w\_Linear}$ ), spectrum method ( $U_{w\_Spectrum}$ ), and JONSWAP method ( $U_{w\_JONSWAP}$ ) at four stations.

waves in very shallow water environments, which is not included in ADV-PUV algorithm. The estimated spectrum by ADV-PUV is different from real wave spectrum (Wu, 1994), and this discrepancy further influences the result of wave orbital velocity.

**Wave orbital velocity and wave-induced shear stress**

Wave orbital velocity calculated by different algorithms ( $U_{w\_Spectrum}$ ,  $U_{w\_Linear}$ ,  $U_{w\_JONSWAP}$ ) and wave-induced shear stress (skin-friction and ripple-related) are shown in Figs. 4 and 5 and Table 2. The  $U_{w\_Linear}$  values were generally larger than  $U_{w\_Spectrum}$  at station T1 (e.g., the tidal cycles from 30 April to 1 May when maximum water level <1 m), mainly due to the nonlinear properties of waves associated with very shallow water. The deviation between  $U_{w\_Linear}$  and  $U_{w\_Spectrum}$  at station T1 can reach 60.3% on average. At station W1, the estimated values of  $U_w$  by different algorithms at the offshore stations were similar, despite some discrepancies between  $U_{w\_JONSWAP}$  and the values based on the other two algorithms.

In order to evaluate the influence of ripples on hydrodynamic process, we took the intertidal station T1 and the offshore station S1 as examples to calculate ripple-related bottom shear stress. Due to the presence of ripples, the values of skin-friction wave shear stress  $\tau_{ws}$  were smaller than ripple-related wave shear stress ( $\tau_{wr\_van}$  and  $\tau_{wr\_GM}$ ) at both stations (Fig. 5). On average,  $\tau_{wr}$  is eight times as large as  $\tau_{ws}$  at T1, and four times as large as  $\tau_{ws}$  at S1. Compared with the offshore station, ripples resulted in a greater increase of bottom shear stress at the intertidal station. The reason is that in the very shallow water area (i.e., intertidal flat), it is much easier for the surface wave energy to penetrate to the bottom, interact with bottom sediments, and be influenced by bedforms. The differences between  $\tau_{wr\_van}$  and  $\tau_{wr\_GM}$  may be due to the different

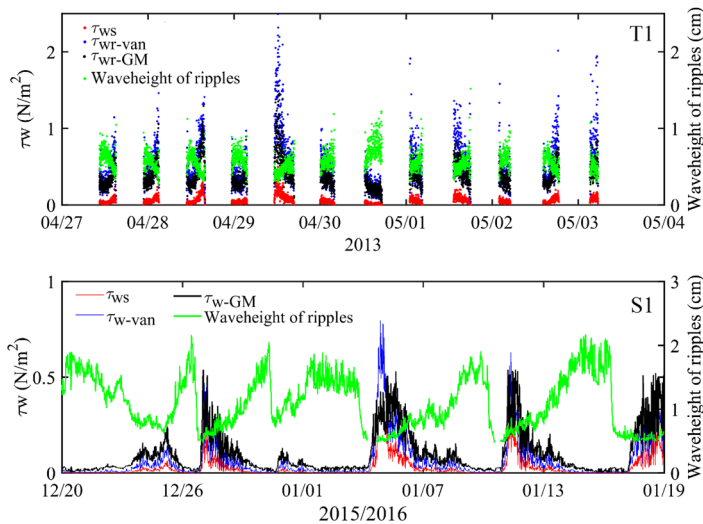


**Fig. 5.** Skin wave-induced shear stress ( $\tau_{ws}$ ), ripple-enhanced wave-induced shear stress ( $\tau_{wr\_van}$ ,  $\tau_{wr\_GM}$ ), and wave height of ripples at station T1 and S1.

**Table 3.** Inter-comparison index of agreement (slope, correlation coefficient (R), root-mean-square error (RMSE), I (Willmott model) and brier skill scores (BSS) between  $U_{w\_Spectrum}$  and  $U_{w\_Linear}$ ,  $U_{w\_Spectrum}$  and  $U_{w\_JONSWAP}$ .

Stations	T1	W1		S1		X1	
	$U_{w\_Spectrum}$ & $U_{w\_Linear}$	$U_{w\_Spectrum}$ & $U_{w\_Linear}$	$U_{w\_Spectrum}$ & $U_{w\_JONSWAP}$	$U_{w\_Spectrum}$ & $U_{w\_Linear}$	$U_{w\_Spectrum}$ & $U_{w\_JONSWAP}$	$U_{w\_Spectrum}$ & $U_{w\_Linear}$	$U_{w\_Spectrum}$ & $U_{w\_JONSWAP}$
Slope	1.45	1.01	0.95	1.03	1.06	1.04	1.04
R	0.77	0.80	0.70	0.97	0.95	0.98	0.96
RMSE	0.06	0.02	0.04	0.02	0.02	0.02	0.03
I*	0.54	0.59	0.66	0.71	0.70	0.71	0.72
BSS†	-1.1	-0.28	0.42	0.92	0.85	0.90	0.95

$$*I = 1 - \frac{\sum (U_{w\_Spectrum} - U_{w\_other})^2}{\sum (|U_{w\_other} - U_{w\_Spectrum}| + |U_{w\_Spectrum} - U_{w\_Spectrum}|)^2}, \quad U_{w\_other} \text{ means } U_{w\_Linear} \text{ or } U_{w\_JONSWAP}$$

$$†BSS = 1 - \frac{\sum (U_{w\_Spectrum} - U_{w\_other})^2}{\sum (U_{w\_Spectrum} - U_{w\_Spectrum})^2}$$

empirical formulae in use and will be further discussed in “The influence of ripples on wave-induced shear stress” section.

## Discussions

### Comparison among different algorithms for wave orbital velocity

To evaluate the validity of different algorithms for wave orbital velocity, especially the linear wave theory method and JONSWAP method, we introduced several indices including slope, correlation coefficient ( $R$ ), root-mean-square error ( $RMSE$ ), index of agreement ( $I$ ), (Willmott et al., 1981; Zhu et al., 2016) and Brier skill scores ( $BSS$ ) (Brier, 1950, Table 3). The index  $I$  varies between 0 and 1, with  $I = 0$  indicating no agreement and  $I = 1$  indicating perfect agreement.  $BSS > 0$  indicates that the values of  $U_{w\_Linear}$  or  $U_{w\_JONSWAP}$  represent a better predictor of  $U_{w\_Spectrum}$  than the average value of  $U_{w\_Spectrum}$ ;  $BSS = 1$  if the agreement is perfect.

There is high agreement among the calculated  $U_w$  using different algorithms at the offshore stations. The scatter plots of  $U_{w\_Spectrum}$  against  $U_{w\_Linear}$  and  $U_{w\_Spectrum}$  against  $U_{w\_JONSWAP}$  are shown in Fig. 6. The correlation coefficients between  $U_{w\_Spectrum}$  and  $U_{w\_Linear}$  (as well as  $U_{w\_Spectrum}$  and  $U_{w\_JONSWAP}$ ) were 0.80 (0.70), 0.98 (0.96), and 0.97 (0.95), for stations W1, X1, and S1, respectively. The slopes for the linear relationship between  $U_{w\_Spectrum}$  and  $U_{w\_Linear}$  (and between  $U_{w\_Spectrum}$  and  $U_{w\_JONSWAP}$ ) were 1.01 (0.95), 1.04 (1.04), and 1.03 (1.06) at stations W1, X1, and S1, respectively. These stations were also associated with low values of  $RMSE$  and high values of  $I$  and  $BSS$  (except for the low  $BSS$  values at W1). The agreement is good in these cases even though the buoy and the tripod are not located at the same depth. Some minor differences (e.g., at W1) existed in the relationship between  $U_{w\_Spectrum}$  and  $U_{w\_Linear}$  when  $T_p < 6$  s (Fig. 4), which is the deep-water wave threshold for a water depth of  $\sim 30$  m ( $T_{deep} = \sqrt{4\pi h/g}$ ) (Wiberg and Sherwood, 2008). As shown in Fig. 2, the differences in

orbital velocity among different wave periods are small in shallow water because orbital velocity becomes dominantly a function of depth ( $U_w = 0.5H(g/h)^{0.5}$  for shallow water) and is not influenced by wave period. When the water becomes deeper with respect to the wavelength of the waves, any single measurement of wave height or period used in Eq. 1 cannot capture the contribution of full wave spectrum to bottom orbital velocity. Thus, the values of  $U_{w\_Linear}$  are somewhat underestimated, i.e., lower than  $U_{w\_Spectrum}$  when  $T_p < 6$  s. Generally, wave orbital velocity calculated by linear wave theory is reasonable at the offshore stations since the waves belonged to a shallow water category for most of the time. In addition, the estimated  $U_w$  values using JONSWAP spectral forms ( $U_{w\_JONSWAP}$ ) also agreed well with  $U_{w\_Spectrum}$  at W1, X1, and S1, except that some low-energy conditions were presented when  $U_{w\_JONSWAP}$  approached zero whereas  $U_{w\_Spectrum}$  remained high (Fig. 4). As suggested by Wiberg and Sherwood (2008), assuming a unimodal spectrum, large errors are likely to occur when JONSWAP method is applied to the wave conditions that are not unimodal in reality. The largest discrepancies between  $U_{w\_Spectrum}$  and  $U_{w\_JONSWAP}$  existed when the measured spectra were bimodal, with the larger peak being associated with higher frequencies. The simple unimodal spectrum may also not well present small wave orbital velocity under low sea-state conditions. Furthermore, JONSWAP formulations assume that waves are traveling in one dominant direction; in this case the wave fields with multiple significant directions will not be well described using the JONSWAP technique. Nevertheless, this technique is particularly useful for defining the  $U_w$  spatial field from significant wave height and peak periods (Wiberg and Sherwood, 2008).

In contrast, a low agreement between linear wave theory and spectrum method was present at the very shallow water station T1, which is mainly due to the nonlinear properties of waves that deviate from the linear wave theory. At T1, the correlation coefficient ( $R = 0.77$ ) and agreement index ( $I = 0.54$ ) between  $U_{w\_Spectrum}$  and  $U_{w\_Linear}$  are smaller than those for

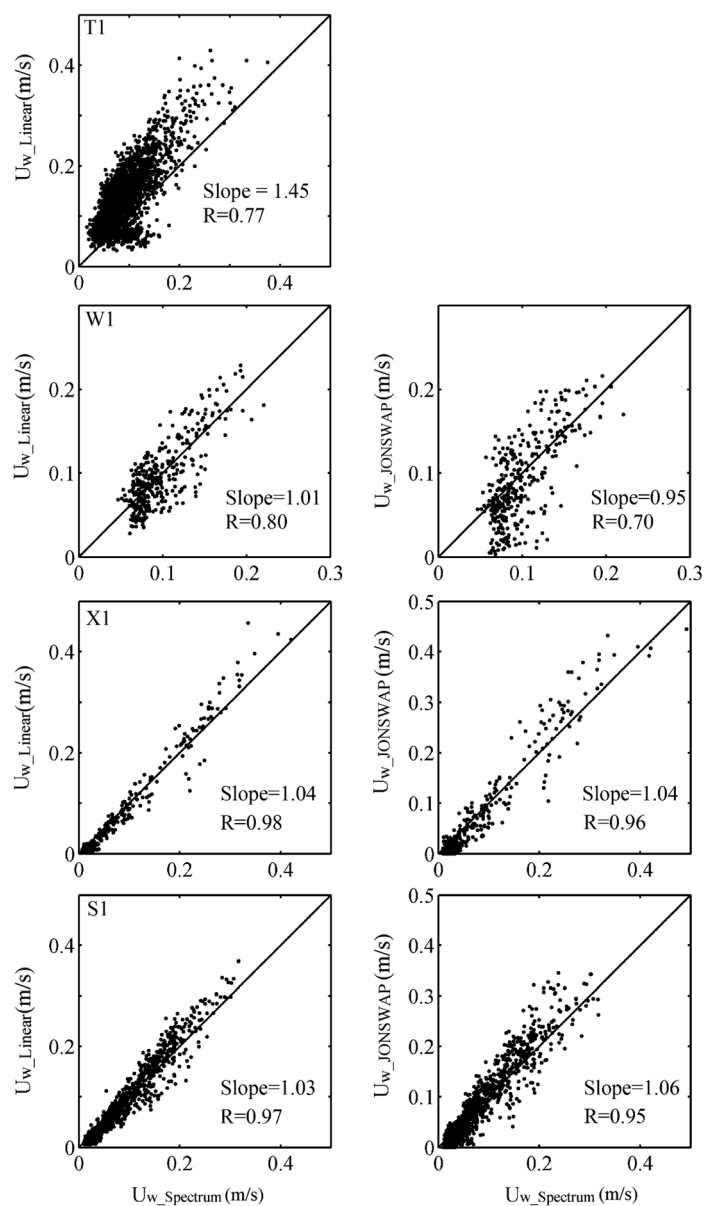


**Fig. 6.** Scatter between wave orbital velocity estimated by spectrum method and linear wave theory, spectrum method and JONSWAP method at all stations.

offshore stations.  $BSS < 0$  means  $U_{w\_Linear}$  is a poor predictor of  $U_{w\_Spectrum}$  than the average value of  $U_{w\_Spectrum}$ . The values of  $U_{w\_Linear}$  were greater than  $U_{w\_Spectrum}$  for most of the time. Figures 3 and 4 show that the major differences between  $U_{w\_Spectrum}$  and  $U_{w\_Linear}$  occurred when maximum water level during a tidal cycle was below 1 m. The  $H_s$  values estimated by ADV-PUV algorithm were greater than those obtained from SBE 26plus for these tidal cycles, resulting in the over-estimation of  $U_{w\_Linear}$  on the intertidal flat. ADV-PUV algorithm uses linear wave theory to convert velocity and pressure spectra to surface elevation spectra (Gordan and Lohrmann, 2002) and it does not include any nonlinear property (Wu, 1994). The estimated

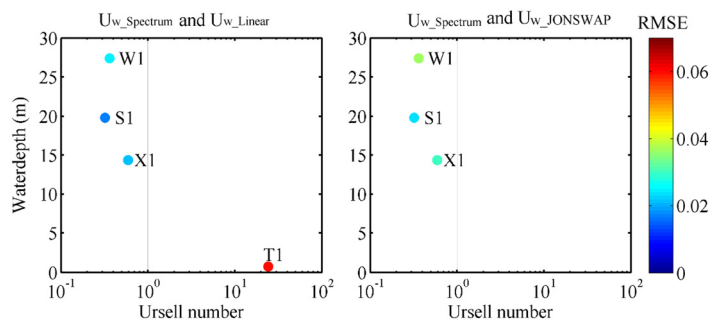


**Fig. 7.** Relationship among Ursell number, water depth, and RMSE. The color denotes the RMSE (root-mean-square error) between spectrum method and linear wave theory (left panel), spectrum method and JONSWAP method (right panel).

spectra by ADV-PUV are little different from field wave spectrum, particularly in shallow water areas (Wu, 1994). The recommended depth of PUV algorithm application is below 50 m (Wu et al., 1996). Moreover, according to the Nortek PUV algorithm application manual, this method is limited to the areas shallower than 10–15 m with a wave period being longer than 4 s. In our results, the ADV-PUV algorithm is suitable for the water depths of 15–30 m, but not for very shallow water conditions (e.g., station T1).

From the viewpoint of *Ursell number*, defined as  $U_R = HL^2/h^3$ , linear wave theory is valid only for relatively small *Ursell number* ( $U_R < 1$  for small wave steepness ( $H/L$ ), cf. SBE 26plus user manual; Ursell, 1953; Kobayashi et al., 1987; Hedges and Ursell, 1995). The average  $U_R$  values were 0.36, 0.59, 0.32, and 24 for W1, X1, S1, and T1, respectively. The relationship among  $U_R$ , water depth, and RMSE were plotted in Fig. 7.

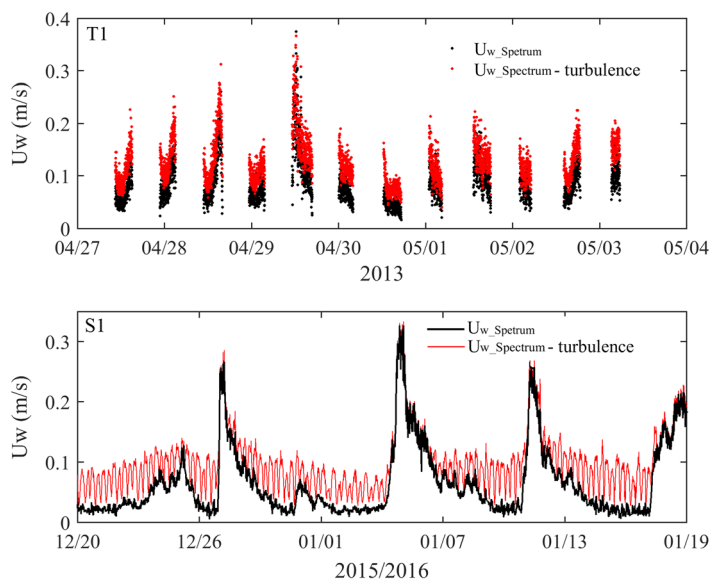


**Fig. 8.** Influence of turbulence on the calculation of wave orbital velocity ( $U_w$ ) when using spectrum method. Black dot (line) denotes  $U_w$  with turbulence removed. Red dot (line) means  $U_w$  influenced by turbulence.

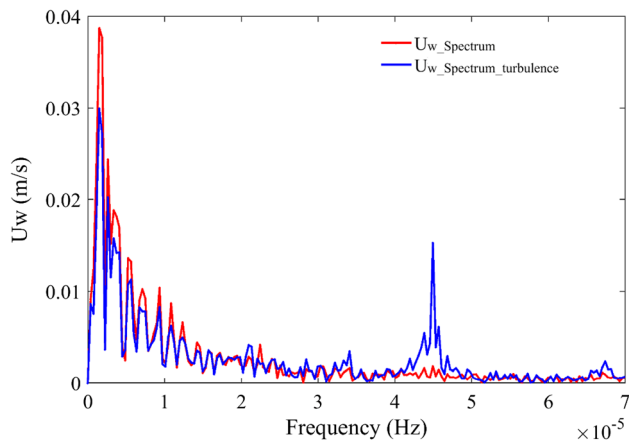


**Fig. 9.** A Fourier analysis of wave orbital velocity ( $U_w$ ) before and after removing turbulence when using spectrum method to obtain  $U_w$ . The red line represents  $U_w$  with turbulence removed ( $U_{w\_Spectrum}$ ). The blue line denotes  $U_w$  under the influence of turbulence ( $U_{w\_Spectrum\_turbulence}$ ). The obvious gap between the red line and the blue line happens at the frequency of  $4.5 \times 10^{-5} \text{ s}^{-1}$  ( $\approx 6.18 \text{ h}$ ), which denotes a M4 component of  $U_{w\_Spectrum\_turbulence}$ .

Clearly, linear wave theory was not suitable for the very shallow intertidal station T1 where  $U_R \gg 1$ . Thus, it is recommended to obtain wave orbital velocity directly from high-frequency velocity measurement (e.g., ADV) and wave parameters (e.g., wave height, wave period) from wave gauge instruments (e.g., SBE 26plus) or zero-crossing algorithm from high-frequency pressure measurement of ADV for very shallow water environments such as intertidal flats. When  $U_R < 1$  (which was the case for the offshore stations), both ADV and buoy instruments can be used to measure wave parameters, and linear wave theory, spectrum and JONSWAP methods are all applicable to estimate wave orbital velocity.

#### The influence of turbulence on the estimation of wave orbital velocity

The frequency overlapping between wave and turbulence will unavoidably result in over-estimation of wave orbital velocity estimation by spectrum method. According to Wiberg and Sherwood (2008),  $U_{w\_Spectrum}$  can also be expressed as  $U_{w\_Spectrum} = \sqrt{2(\text{var}(u') + \text{var}(v'))}$ , where  $u' = u - \langle u \rangle$ ,  $v' = v - \langle v \rangle$  (" $\langle \rangle$ " denotes average value) are components of instantaneous velocity. Since  $u' = u_{\text{wave}} + u_{\text{turbulence}}$ , the term  $\text{var}(u')$  ( $=\text{var}(u_{\text{wave}}) + \text{var}(u_{\text{turbulence}})$ ) includes variations of both waves and turbulence. When turbulence is included, the results of  $U_{w\_Spectrum\_turbulence}$  are overestimated and present salient tidal signal in phase with the current (M4 variation), especially for station S1 (deployed for a whole month from 20 Dec 2015 to 19 Jan 2016) (Fig. 8). In present study, values of  $U_{w\_Spectrum\_turbulence}$  were obtained for every 1 min (station T1), 30 min (station W1), 10 min (station X1), and 20 min (station S1). Though turbulence is also associated with the wave boundary itself, the period of wave is usually 1–10 s and



**Fig. 10.** Ripple scales of field measurements in May 2017 at Dafeng tidal flat, which is close to station T1.

the influence of wave on the variation of  $U_{w\_Spectrum\_turbulence}$  could be filtered by burst-averaging. Therefore, the M4 variation of  $U_{w\_Spectrum\_turbulence}$  is mainly due to turbulence levels increasing/decreasing with tidal current strength.

To remove the influence of turbulence, the turbulence spectrum is first calculated by energy spectrum analysis (Soulsby and Humphery, 1990; Zhu et al., 2016) and then subtracted from the whole spectrum ( $u_{\text{wave}} + u_{\text{turbulence}}$ ). The frequency of turbulence and wave interact with each other during certain range (Bricker and Monismith, 2007), so the influence of turbulence cannot be totally removed due to the limitation of the method. The results of present study turn out to be satisfactory and in good agreement with  $U_{w\_Linear}$  and  $U_{w\_JONSAWP}$  (Fig. 4). Taking station S1 as an example, the Fast Fourier Transform analysis result of  $U_w$  time series before and after removing turbulence (Fig. 9) shows an obvious gap between  $U_{w\_Spectrum}$  and  $U_{w\_Spectrum\_turbulence}$  at the frequency of  $4.5 \times 10^{-5} \text{ s}^{-1}$  ( $\approx 6.18 \text{ h}$ ), denoting M4 components of  $U_{w\_Spectrum\_turbulence}$ . The Fourier result also demonstrates that the influence of turbulence on bottom wave orbital velocity has been almost cleared.

#### The influence of ripples on wave-induced shear stress

Bottom roughness is an important parameter in many hydrodynamic and morphodynamic models for lakes, estuaries, and coastal waters (Wiberg and Sherwood, 2008). Wave motion induced shear stress can lead to mobilization of bed sediment, which can further alter the bottom roughness, e.g., through formation or elimination of small-scale ripples. Such ripples in turn modify wave energy dissipation and bottom drag for bottom boundary layer flows. Ripples in coastal areas reach a particular height or length dependent on the particle size ( $d_{50}$ ), wave period ( $T_p$ ), and peak near bed orbital velocity ( $U_w$ ) (van Rijn, 2007). At station T1, the calculated wave height of ripples based on Eqs. 10 and 11 is in the range of 0.27–1.16 cm (with an average of 0.48 cm). These scales are comparable to our field measurements in May 2017 on the

Dafeng tidal flat (Fig. 10) and the results of Zhao et al., (2012) at Dongtai and Gao (2009) at Wanggang, adjacent to station T1. The calculated wave height of ripples at station S1 ranged between 0.40 and 2.17 cm (with an average of 1.08 cm, Fig. 5). Since it was difficult to observe the ripple dimension at the seabed, especially within the turbid water at high water periods, these calculated wave heights of ripples were only used as a preliminary index to investigate the ripple influence on the bottom wave-induced shear stress.

The ripple-related bottom shear stress ( $\tau_{wr\_van}$ ,  $\tau_{wr\_GM}$ ) is much larger than the skin-friction shear stress  $\tau_{ws}$  (Fig. 5). At station T1, values of  $\tau_{wr\_van}$  and  $\tau_{wr\_GM}$  were close to each other except for tide 5; maximum  $\tau_{wr\_van}$  reached up to 2.17 N m<sup>-2</sup>. However, at station S1,  $\tau_{wr\_GM}$  was larger than  $\tau_{wr\_van}$  for almost the entire measurement period. Primary analysis concerned with these two models shows that: (1) the GM model relates the ripple-related roughness height ( $k_{br}$ ) directly with the ripple height/length, while the van Rijn model combines  $k_{br}$  with median grain size of silt and gravel (here we propose that the former would be more reasonable for estimating  $k_{br}$  by directly linking with the ripple dimension); and (2) the ripple dimension was merely calculated by empirical formulae, which may not be applicable to the offshore stations. Here we recommend that in situ measurements, such as Acoustic Ripple Profiler (Bolaños et al., 2012), should be carried out to obtain the ripple information and compare with empirical formulae. In addition, the distance from the ADV probe to the seabed, which was registered at the beginning or end of every burst, can also be used to estimate ripple or morphology evolution at a fixed point (Pratolongo et al., 2010). According to our field-work experience, however, the ADV probes should be deployed close to the bed (i.e., within 0.3 m) in order to record such data sets, which maybe a risk for the probe safety, especially in offshore areas.

## Conclusion

Bottom wave orbital velocity has been calculated by different algorithms depending on the datasets available at four stations, with one in intertidal flat with depth being around 1 m and the remainder three in offshore deeper waters with depths of 15–30 m. The spectrum method and linear wave theory are in good agreement for the offshore sites, despite a minor gap between these two algorithms when  $T_p < 6$  s (the deep-water wave threshold for a water depth of ~30 m). In the absence of near-bed high-frequency velocity measurements, bottom orbital velocity can be estimated using significant wave height and peak period to parameterize a general spectral form (e.g., JONSWAP spectral forms), thereby producing an approximate surface-wave height spectrum. Estimated  $U_w$  using JONSWAP spectral forms also agrees well with bottom wave orbital velocity by spectrum method. Thus, it is reasonable to use any of the three algorithms and to use different instruments measuring at different water depths to calculate wave

orbital velocity in offshore waters. However, significant discrepancies exist among different datasets and different algorithms for the intertidal site. The correlation between spectrum method and linear wave theory is weaker at the very shallow intertidal area, due to the deviation from the nonlinear property assumption. Thus, it is recommended to use measured high-frequency velocity to calculate wave orbital velocity and to use wave gauge instrumentation or zero-crossing algorithm, rather than PUV algorithm, to obtain wave height/period. In addition, to avoid the tide modulated orbital velocity tendency, the impact of turbulence should be removed for the spectrum method. Where ripples are present, the ripple-related wave shear stress tends to be much larger than the skin-friction shear stress. Ripples on the intertidal flat can cause a significant increase in near-bed shear stress than in offshore areas.

## References

- Allen, J. R. 1970. Physical processes of sedimentation. London: Unwin Univ. Books, p. 248.
- Biron, P. M., C. Robson, M. F. Lapointe, and S. J. Gaskin. 2004. Comparing different methods of bed shear stress estimates in simple and complex flow fields. *Earth Surf. Process. Landforms* **29**: 1403–1415.
- Bolaños, R., P. D. Thorne, and J. Wolf. 2012. Comparison of measurements and models of bed stress, bedforms and suspended sediments under combined currents and waves. *Coastal Eng.* **62**: 19–30.
- Boyd, R., D. Forbes, and D. Heffler. 1988. Time-sequence observations of wave-formed sand ripples on an ocean shoreface. *Sedimentology* **35**: 449–464.
- Bricker, J. D., and S. G. Monismith. 2007. Spectral wave-turbulence decomposition. *J. Atmos. Oceanic Technol.* **24**: 1479–1487.
- Brier, G. W. 1950. Verification of forecasts expressed in terms of probability. *Mon. Weather Rev.* **78**: 1–3.
- Davis, J. P., D. J. Walker, M. Townsend, and I. R. Young. 2004. Wave-formed sediment ripples: transient analysis of ripple spectral development. *J. Geophys. Res. Oceans* **109**(C07020). doi:10.1029/2004JC002307
- Donelan, M. A., J. Hamilton, and W. H. Hui. 1985. Directional spectra of wind-generated waves. *Philos. Trans. R. Soc., London A: Math., Phys. Eng. Sci.* **315**: 509–562.
- Dong, L. X., W. B. Guan, Q. Chen, X. H. Li, X. H. Liu, and X. M. Zeng. 2011. Sediment transport in the Yellow Sea and East China Sea. *Estuarine, Coastal Shelf Sci.* **93**: 248–258.
- Gao, S. 2009. Modeling the preservation potential of tidal flat sedimentary records, Jiangsu coast, eastern China. *Cont. Shelf Res.* **29**: 1927–1936. doi:10.1016/j.csr.2008.12.010
- Gordon, L., and A. Lohrmann. 2002. Near-shore Doppler current meter wave spectra. *Proc. Fourth Int. Symp. on Ocean Wave Measurement and Analysis, WAVES2001*, San Francisco, CA, ASCE, 33–43.

- Goring, D. G., and V. I. Nikora. 2002. Despiking acoustic Doppler velocimeter data. *J. Hydraul. Eng.* **128**: 117–126.
- Grant, W. D., and O. S. Madsen. 1982. Movable bed roughness in unsteady oscillatory flow. *J. Geophys. Res. Oceans* **87**: 469–481.
- Hasselmann, K., T. Barnett, E. Bouws, H. Carlson, D. Cartwright, K. Enke, J. A. Ewing, and H. Gienapp, and others. 1973. Measurements of wind-wave growth and swell decay during the joint north sea wave project (JONSWAP). Deutsches Hydrographisches Institut.
- He, X. Y., T. Hu, Y. P. Wang, X. Q. Zou, and X. Z. Shi. 2010. Seasonal distributions of hydrometeor parameters in the off-shore sea of Jiangsu. *Mar. Sci.* **34**: 44–54 (in Chinese with English abstract).
- Hedges, T. S., and URSELL. 1995. Regions of validity of analytical wave theories. *Proc. Inst. Civ. Eng.-Water Marit. Energy* **112**: 111–114.
- Jonsson, I. G. 1967. Wave boundary layers and friction factors, p. 127–148. *In* Proceedings of Conference in Coastal Engineering, Tokyo.
- Kim, S. C., C. Friedrichs, J. Y. Maa, and L. Wright. 2000. Estimating bottom stress in tidal boundary layer from acoustic Doppler velocimeter data. *J. Hydraul. Eng.* **126**: 399–406.
- Kobayashi, N., A. K. Otta, and I. Roy. 1987. Wave reflection and run-up on rough slopes. *Journal of Waterway, Port, Coastal, and Ocean Engineering*, **113**(3): 282–298.
- Li, M. Z., and C. L. Amos. 1998. Predicting ripple geometry and bed roughness under combined waves and currents in a continental shelf environment. *Cont. Shelf Res.* **18**: 941–970.
- Li, M. Z., and C. L. Amos. 2001. Sedtrans96: the upgraded and better calibrated sediment-transport model for continental shelves. *Comput. Geosci.* **27**: 619–645.
- Lu, Y. Z., J. X. Wu, and H. Liu. 2012. An integrated post-processing technique for turbulent flows in estuarine bottom boundary layer. *Acta Oceanol. Sin.* **34**: 39–49 (in Chinese with English abstract).
- MacIsaac, C., and Naeth, S. 2013. TRIAXYS next wave II directional wave sensor - the evolution of wave measurements, p. 1–8. *In* 2013 OCEANS - San Diego, 2013 (pp. 1–8). IEEE.
- Nielsen, P. 1979. Some basic concepts of wave sediment transport, Vol. 20 of Series Paper. *Inst. of Hydrodynamics and Hydraulic Engineering*, ISVA, Tech. Uni. of Denmark. First ed.
- Nielsen, P. 1992. Coastal bottom boundary layers and sediment transport, v. **4**. World Scientific Publishing Company.
- Nikuradse, J. 1932. Laws of turbulent flow in smooth pipes. VDI, p. 359 English translation NACA TTF-10, 1950.
- Pierson, W. J., and L. Moskowitz. 1964. A proposed spectral form for fully developed wind seas based on the similarity theory of S. A. Kitaigorodskii. *J. Geophys. Res.* **69**: 5181–5190.
- Pratolongo, P. D., G. M. E. Perillo, and M. C. Piccolo. 2010. Combined effects of waves and plants on a mud deposition event at a mudflat-saltmarsh edge in the Bahía Blanca Estuary. *Estuarine, Coastal Shelf Sci.* **87**: 207–212.
- Sobey, R. J., and S. A. Hughes. 1999. A locally nonlinear interpretation of PUV measurements. *Coastal Eng.* **36**: 17–36.
- Soulsby, R. L. 1987. Calculating bottom orbital velocity beneath waves. *Coastal Eng.* **11**: 371–380.
- Soulsby, R. L. 1997. Dynamics of marine sands: a manual for practical applications. Thomas Telford, London.
- Soulsby, R. L., and J. Humphery. 1990. Field observations of wave-current interaction at the sea bed *Water wave kinematics*. Springer, p. 413–428.
- Soulsby, R. L., and J. V. Smallman. 1986. A direct method of calculating bottom orbital velocity under waves. *Hydraulics Research Limited, Report SR 76*, 14pp.
- Soulsby, R. L., and R. J. S. Whitehouse. 2005. Prediction of ripple properties in shelf seas, Rep. TR 154, *Hydraul. Res., Ltd.*, Wallingford, U. K.
- TRIAXYS™ OEM Directional Wave Sensor user's manual, 2009. AXYS Technologies Inc.
- Ursell, F. 1953. The long-wave paradox in the theory of gravity waves. *In* Mathematical Proceedings of the Cambridge Philosophical Society (Vol. 49, No. 4, pp. 685–694). Cambridge University Press.
- Van Rijn, L. C. 2007. Unified view of sediment transport by currents and waves. I: initiation of motion, bed roughness, and bed-load transport. *J. Hydraul. Eng.* **133**: 649–667.
- Wiberg, P. L., and C. R. Sherwood. 2008. Calculating wave-generated bottom orbital velocities from surface-wave parameters. *Comput. Geosci.* **34**: 1243–1262.
- Williams, J. J., P. S. Bell, and P. D. Thorne. 2005. Unifying large and small wave-generated ripples. *J. Geophys. Res. Oceans*, **110**(C02008). doi:10.1029/2004JC002513
- Willmott, C. J. 1981. On the validation of models. *Phys. Geogr.* **2**: 184–194.
- Wilson, W. D. and E. Siegel. 2011. Current and wave measurements in support of the Chesapeake Bay interpretive buoy system, p. 94–99. *In* 2011 IEEE/OES 10th current, waves and turbulence measurements (CWTM). IEEE.
- Wu, Z. 1994. Estimate approached of  $\eta$ UV, PUV and UV directional wave spectra and their comparison. *Ocean Eng.* **12**: 79–86 (in Chinese with English abstract).
- Wu, Z., H. S. Zhong, and Y. X. Yan. 1996. Data processing approach of the estimation of directional wave spectra by pressure and water velocity. *Ocean Eng.* **1**: 40–47 (in Chinese with English abstract).
- Yang, B., W. B. Feng, and Y. Zhang. 2014. Wave characteristics at the south part of the radial sand ridges of the southern yellow sea. *China Ocean Eng.* **28**: 317–330.
- Yu, Q., Y. Wang, B. Shi, Y. P. Wang, and S. Gao. 2017. Physical and sedimentary processes on the tidal flat of Central Jiangsu coast, China: headland induced tidal eddies and benthic fluid mud layers. *Cont. Shelf Res.* **133**: 26–36.
- Zhao, N., X. J. Liu, and G. Lu. 2012. Characteristics and evolution process and their modeling of sand ripples on Dongtai

tidal flats, Jiangsu Province China. *J. Sediment Res.* **3**: 004 (in Chinese with English abstract).

Zhu, Q., B. van Prooijen, Z. Wang, Y. Ma, and S. Yang. 2016. Bed shear stress estimation on an open intertidal flat using in situ measurements. *Estuarine, Coastal Shelf Sci.* **182**: 190–201.

#### Acknowledgments

We thank Shi BW, Chen DZ, Lu HH, Zhu QG, Cheng GL, Chen DX, and Ji CC for their assistance in the field work and laboratory measurements. Finally, we wish to thank the two anonymous reviewers and the associated editor Dr. Craig Lee, who helped to greatly improve the manuscript. This study was supported by the National Natural Science Foundation of China (41625021), Marine Science and Technology Innovation

Program of Jiangsu Province (HY2017-2), and the Laboratory for Marine Geology, Qingdao National Laboratory for Marine Science and Technology (MGQNLN-KF201714).

#### Conflict of interest

None declared.

*Submitted 6 December 2017*

*Revised 3 May 2018*

*Accepted 11 July 2018*

*Associate editor: Craig Lee*